Improving U-Net Confidence on TEM Image Data with L2-Regularization, Transfer Learning, and Deep Fine-Tuning

Aiden Ochoa   Xinyuan Xu   Xing Wang*

Penn State University

{aio5165, xkx5062, xvw5285}@psu.edu

Abstract

With ever-increasing data volumes, it is essential to develop automated approaches for identifying nanoscale defects in transmission electron microscopy (TEM) images. However, compared to features in conventional photographs, nanoscale defects in TEM images exhibit far greater variation due to the complex contrast mechanisms and intricate defect structures. These challenges often result in much less labeled data and higher rates of annotation errors, posing significant obstacles to improving machine learning model performance for TEM image analysis. To address these limitations, we examined transfer learning by leveraging large, pre-trained models used for natural images.

We demonstrated that by using the pre-trained encoder and L2-regularization, semantically complex features are ignored in favor of simpler, more reliable cues, substantially improving the model performance. However, this improvement cannot be captured by conventional evaluation metrics such as F1-score, which can be skewed by human annotation errors treated as "ground truth". Instead, we introduced novel evaluation metrics that are independent of the annotation accuracy. Using grain boundary detection in UO_2 TEM images as a case study, we found that our approach led to a 57% improvement in defect detection rate, which is a robust and holistic measure of model performance on the TEM dataset used in this work. Finally, we showed that model self-confidence is only achieved through transfer learning and fine-tuning of very deep layers.

1. Introduction

Nanoscale defects, such as grain boundaries, precipitates, and dislocations, play a critical role in controlling the properties and functionality of solid-state materials. Transmission electron microscopy (TEM) has become an irreplaceable tool for investigating these defects, owing to its ultrahigh spatial resolution (sub-Angstrom) [16]. Furthermore, recent advances in faster electron detection and data processing have enabled a big-data approach to characterization techniques such as in-situ TEM and 4D-scanning transmission electron microscopy (4D-STEM) [8]. Terabytes of data can be created in a single hour during 4D-STEM or in-situ TEM experiments [5]. However, extracting meaningful insights from the data has quickly become an enormous bottleneck, since the traditional method of manual image analysis is time-consuming, subject to human bias, and cannot scale with the growing data volume [11]. Therefore, developing high-quality automated approaches for TEM image analysis is of paramount importance.

Since the discovery of convolutional neural networks (CNN), machine learning (ML) models have been able to outperform not only traditional computer vision techniques, but even human abilities on certain image analysis tasks [7]. In the context of TEM, binary segmentation utilizing models from the U-Net family enables pixel-level classification of defect structures, which is especially important for identifying continuous defects like grain boundaries and phase interfaces [10]. However, comparing applications to more typical datasets, the performance of CNN models for TEM image analysis remains inferior. For instance, most of the literature involving U-Net based models, including the seminal paper [9] and popular derivatives like U-Net++ [21], is focused on medical imaging [9]. With these datasets, it is very common to see F1-scores in the range 0.85–0.95. Similar performance can also be seen in applications like forestry [14], crack detection [6], satellite imaging [2], and plant disease [15]. TEM applications, however, usually report lower F1-scores in range 0.5–0.8 [1].

One key reason for this performance gap stems from the inherent complexity of TEM image analysis. Unlike optical images, contrast in TEM arises from multiple mechanisms, making feature identification highly sensitive to imaging conditions and sample characteristics. Consequently, TEM datasets differ from conventional ML datasets in two major ways. (1) Smaller dataset size. TEM datasets typically contain tens to hundreds of labeled images due to the time-intensive nature of annotation. In contrast, datasets like Im-
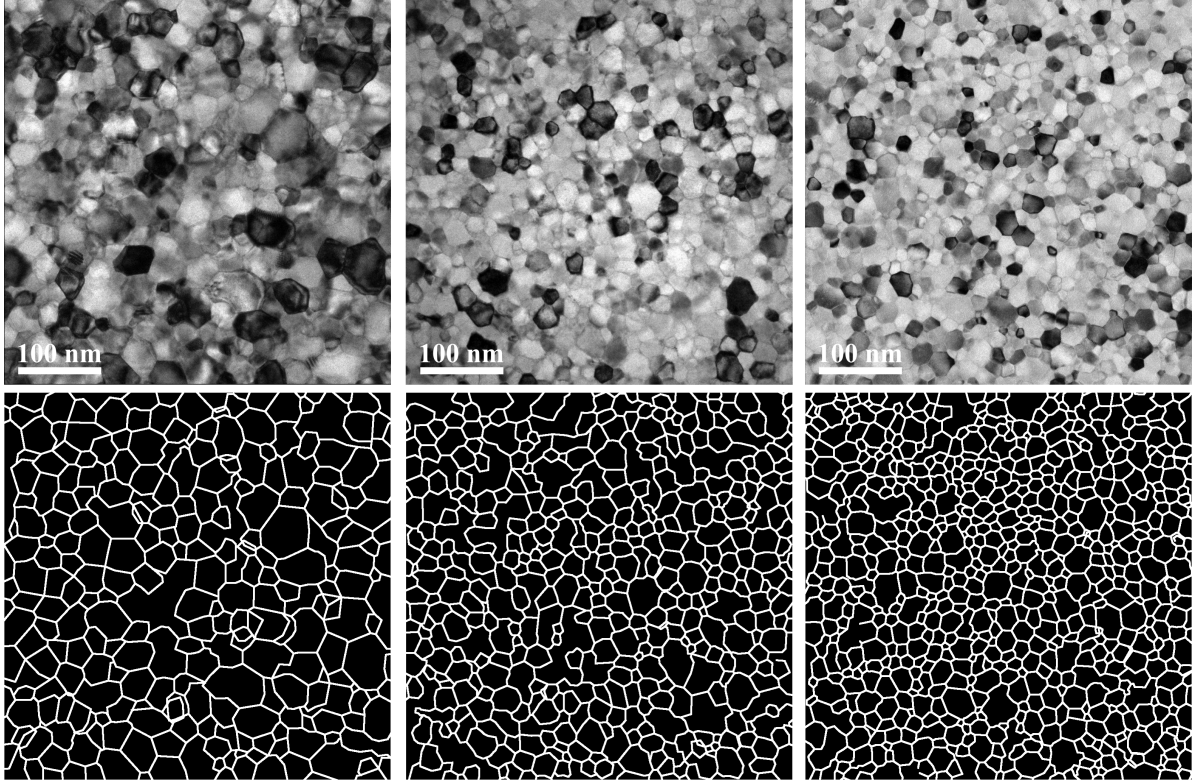
---

*Corresponding Author

Figure 1. Representative TEM images of nanocrystalline UO2 (top) with corresponding annotated grain boundaries (bottom) from the dataset used in this work

ageNet [4] contain more than 14 million annotated images. (2) Greater annotation ambiguity. The complex contrast mechanisms and intricate defect structures often result in large variations in how these defects appear in TEM images. This makes it challenging to annotate all defects within the images, leading to considerable uncertainty and inconsistency in human-labeled data, which is nonetheless treated as "ground truth" during ML model training [3].

To address these challenges, we explored the use of transfer learning by leveraging advanced ML models pre-trained on large datasets for use with TEM analysis. In particular, we investigated promising combinations of a pre-trained EfficientNet encoder with a U-Net++ decoder, which helped achieve the best performance in 2023 and 2024 for edge detection in regular optical image datasets [19][20]. We also introduced two novel metrics, prediction certainty and prediction abundance, describing the ability of a model to make predictions with high class probabilities. Together, they define a model's self-confidence and are independent of ground truth accuracy. We demonstrated that U-Net performance can be substantially improved using a pre-trained encoder, fine-tuning of deep layers, and L2-regularization. Although F1-scores remained limited due to ground truth flaws and uncertainty, improved model self-confidence led to a 57% in-

crease in the number of detected defects for the dataset tested, significantly enhancing the accuracy of defect statistics.

As a practical example, we applied our workflow to a TEM image dataset of nanocrystalline UO_2 samples used to study grain growth as function of temperature and heavy ion irradiation dose. UO_2 is the primary fuel used in current nuclear reactors, and many of its key material properties, such as thermal conductivity, fission gas retention, and fracture toughness, are governed by grain size. Therefore, it is critical to establish reliable correlations between grain size of UO_2 and its irradiation conditions for predictive modeling of nuclear fuel performance. The accuracy of said correlations principally depends on the quality of grain statistics, which in turn requires large and representative datasets. As such, hundreds of TEM images like those in Fig. 1 were collected at various dose levels and temperatures. Processing these images by hand is infeasible, so U-Net models were used to automate segmentation of grain boundaries.

2. Methodology

2.1. Grain Boundary Dataset

The dataset used in this work consists of bright-field (BF) TEM images of nanocrystalline thin-film UO2 samples. De-
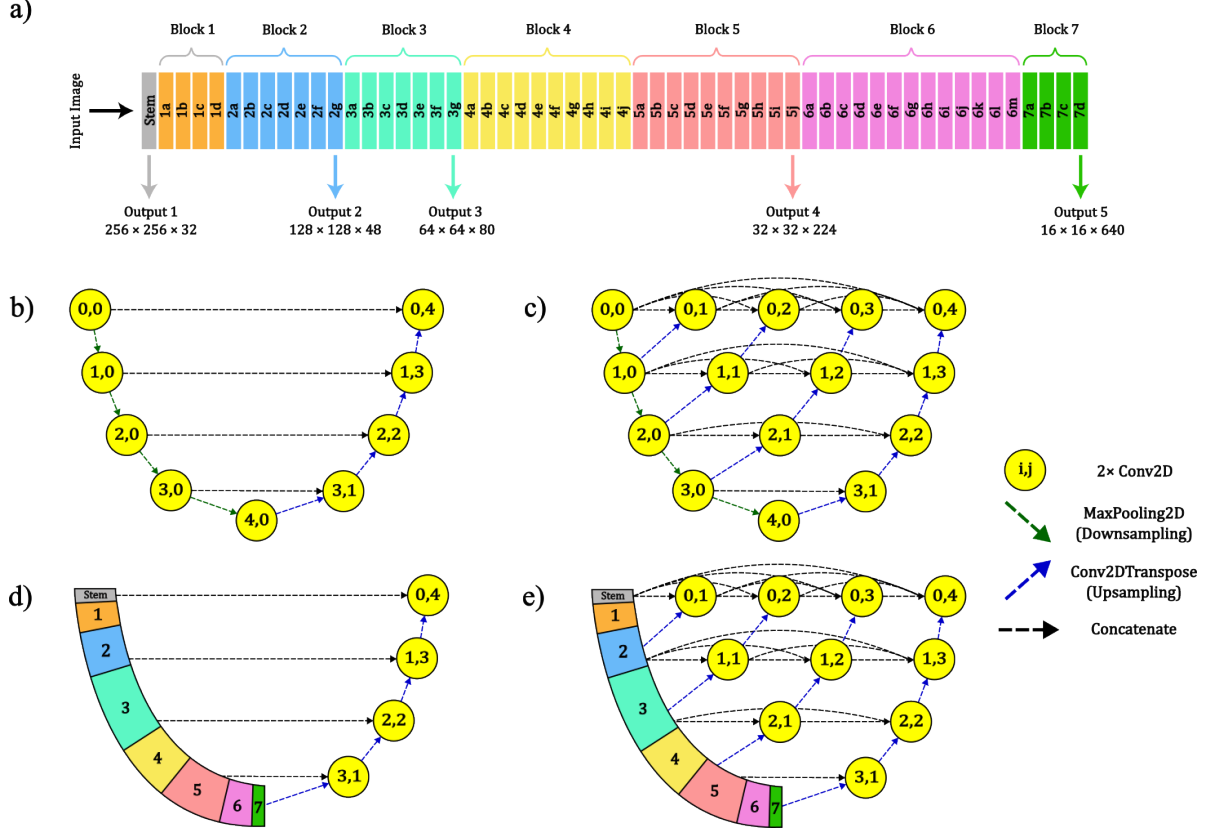
Figure 2. Model architectures evaluated. a) EfficientNetB7 (64M parameters) with 56 convolution layers. b) U-Net (31M) baseline architecture. c) U-Net++ (36M) with intermediate convolution blocks and dense connections. d) U-Net with an EfficientNetB7 backbone (72M). e) U-Net++ with an EfficientNetB7 backbone (76M)

tails about fabrication, in-situ irradiation, and TEM imaging can be found in [18] [17]. The training dataset was created by selecting 14 images from a variety of experimental conditions and resizing them from 4096×4096 to 1024×1024. The grain boundaries were then labeled using Inkscape with a thickness of 5 pixels. Pixels belonging to a grain boundary were given a value of 1, while pixels belonging to the grain interior were given a value of 0. A one-to-one mapping is ultimately constructed between TEM and annotated images. Examples can be seen in Fig. 1.

Small dataset size can lead to significant variation in model performance when different validation and test holdout sets are used. To improve their representation of the training set, each image was quartered into four 512×512 images, and 5-fold cross-validation was used. This divides the dataset into five non-overlapping validation sets of equal size, training a model for each one with the same hyperparameters. Statistics can then be calculated for performance metrics, providing a more robust estimate. This also means a test set is not necessary, further improving validation set representation. To improve model performance, training images were augmented eightfold using 90° rotations and flipping

over horizontal and vertical axes. Each model thus used a different combination of 360 training images and 11 validation images.

2.2. Model Architectures and Hyperparameters

To improve U-Net segmentation performance, the encoder is replaced with EfficientNetB7, the largest model from the EfficientNet-v1 family [13], and the decoder has been replaced with U-Net++. Most promisingly, the architecture EfficientNetB7-U-Net++ has been used as the base network of state-of-the-art edge detectors UAED [19] and MUGE [20], which are applicable to grain boundary segmentation. Furthermore, EfficientNetB7 has been pre-trained on ImageNet [4] to ease training and boost encoder performance for small datasets. This is the sole focus of Sec. 4, where the benefits of transfer learning and fine-tuning are evaluated. EfficientNetB7 and U-Net++ were also isolated to show their respective contributions, leading to the four architectures investigated in this study, as summarized in Fig. 3: UNet (b), UNet++ (c), Eff-UNet (d), and Eff-UNet++ (e).

The Adam optimizer was used with a global learning rate of 1e-4 and a batch size of 4. For the yellow convolution

3

blocks in Fig. 2b-e, each Conv2D layer learned $2^{(i+6)}$ filters, where $i = 0, 1, 2, 3, 4$ refers to the encoder resolution level. ReLU activation was used for all layers except the output layer which used Sigmoid activation. To suppress overfitting, L2-regularization was used to penalize large weights in favor of a more distributed network. The total loss can be written symbolically as

$$\mathcal{L} = \text{BCE}(\text{prediction}, \text{annotation}) + \lambda ||\mathbf{w}||^2,$$

where BCE is binary cross-entropy loss, commonly used in binary segmentation, $\mathbf{w}$ is a vector of model weights, and λ is the L2-regularization strength. In preliminary testing, it was found λ can have substantial effects on model output, specifically on model self-confidence. Given that the architectures in Fig. 2 have different sizes and connections, and thus very different $\mathbf{w}$, a coarse grid search was performed to determine the optimal λ. This grid search provided the basis for model comparison.

2.3. Performance Metrics

To evaluate model performance, classification metrics precision, recall, and F1-score were used with a binarization threshold of 0.5. This minimizes precision-recall tradeoff and maximizes F1-score. Two novel metrics, prediction certainty and abundance, were also used to evaluate model self-confidence. As shown in Fig. 3, they operate on raw prediction image histograms, where certainty measures the ability of a model to predict high class probabilities, and abundance measures the proportion of said pixels that are positive predictions. A model with high certainty tends to avoid uncertain predictions where a pixel could belong to either a grain boundary or non-grain boundary with nearly equal probability. A model with high abundance tends to predict more grain boundaries overall, which is important for

an imbalanced dataset. We describe model self-confidence comparatively as the possession of both certainty and abundance, which, importantly, do not rely on the existence of a ground truth.

The final metric, grain detection rate, was used to provide a holistic measure of model usefulness. It implicitly depends on all other metrics evaluated, as a model must have good classification performance and self-confidence to predict well-defined grains that can be detected by a post-processing algorithm. Models with the highest grain detection rate provide the most accurate grain statistics, and are therefore of supreme practical value. To detect grains from segmented TEM images, we used an algorithm developed in previous work called Convex Hull Approximate Contour (CHAC). CHAC is based on thermodynamics principles stating that grain boundaries should be convex with respect to each other, so only closed convex contours in the processed TEM images should be counted as grains.

3. Results and Discussion

3.1. Visual Comparison of Predictions

Initial insights into model performance can be gained by examining raw model predictions visually. A representative validation prediction is shown for all architectures and L2-regularization strengths in Fig. 4. When no regularization was used, all architectures appeared to perform similarly. However, upon increasing λ, UNet and UNet++ responded quite differently than Eff-UNet and Eff-UNet++. The latter architectures exhibited greater tolerance to regularization, as over-regularization occurred at much higher λ values. Furthermore, predictions made near λ=1e-3 demonstrated significant quality improvements, where models clearly predict higher class probabilities, and thus have greater certainty.
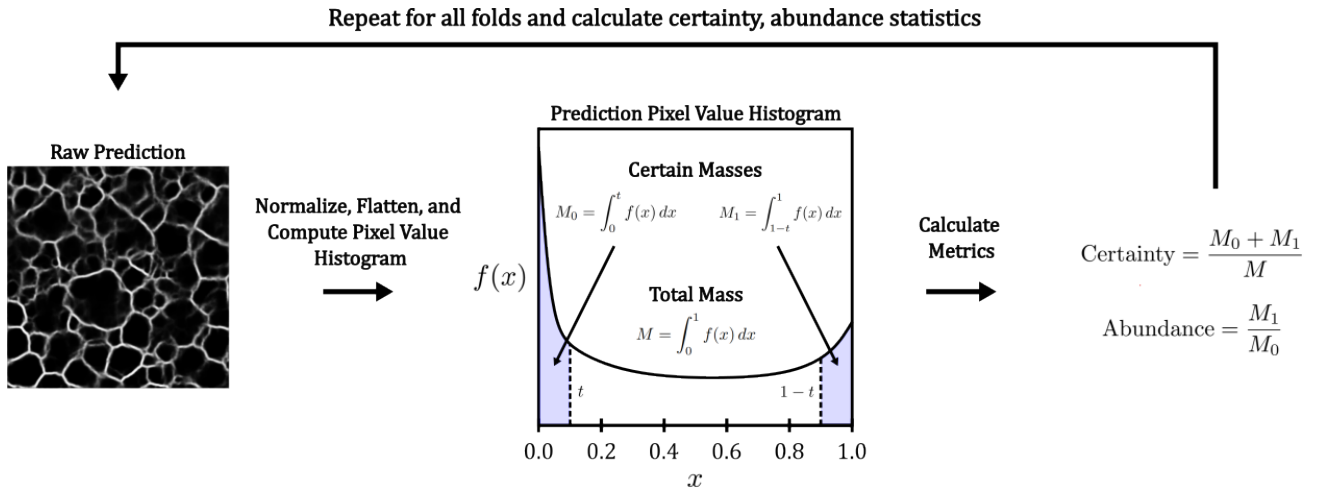

Figure 3. Proposed metrics, certainty and abundance, calculated from pixel value histograms of raw model predictions. The confidence threshold t=0.15 was used in this work
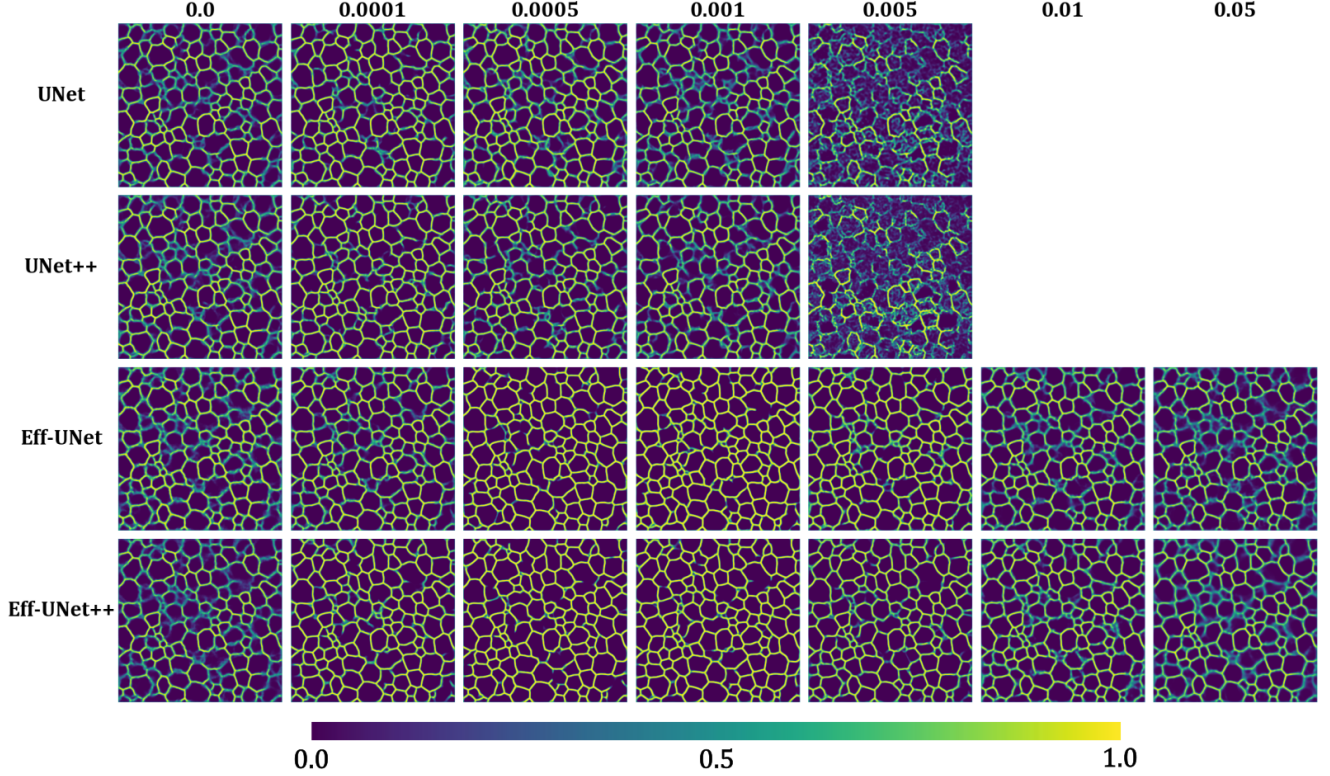
Figure 4. Comparison of raw validation predictions by U-Net architecture and L2-regularization strength λ for a representative TEM input image

This has the primary benefit of reducing grain boundary noise in binarized predictions, as pixel values tend to be far from the threshold (0.5), and are thus not left up to meaningless noise. Finally, unlike changing the encoder, there was no obvious difference between using U-Net and U-Net++ decoders.

3.2. Model Architectures and Hyperparameters

Fig. 5 summarizes the six metrics used to evaluate model architectures for different values of λ. Like the visual results in Fig. 4, architectures behave similarly when $\lambda=0$, other than Eff-UNet and Eff-UNet++ having marginally lower precision and recall. As λ is increased, recall, certainty, abundance, and grain detection rate reached their maximum at $\lambda=$1e-4 for UNet and UNet++, and between $\lambda=$5e-4 and $\lambda=$1e-3 for Eff-UNet and Eff-UNet++. Coincidentally, precision reached its minimum at these points. Furthermore, the following observations can be made: (1) F1-score showed little-to-no improvement despite considerable improvement to grain detection rate, (2) there is a large divergence between U-Net and EfficientNet encoder architectures, with the latter showing much greater certainty, abundance, and grain detection rates in Figs. 5d-f, and (3) given the width of the error bars, there is no practical benefit from using the

U-Net++ decoder.

Most significantly, by using EfficientNet and L2-regularization, grain detection rate increased by 57% over unregularized UNet. For the 14 TEM images in this dataset, that is a difference of 2000 grains, or about 150 more grains detected per image. This is clearly captured by certainty and abundance, but the classification metrics in Figs. 5a-c do not explicitly show this, other than a 7% improvement to recall. This highlights the value of model self-confidence and holistic metrics like grain detection rate. As discussed next in Sec. 3.3, the tradeoff between precision and recall as λ increases does provide some insight, but F1-score may not be entirely reliable for images that have annotation errors.

3.3. Importance of L2-Regularization

As shown in Fig. 5c, the F1-score is limited to 0.75, regardless of architecture or regularization strength. To investigate this limitation, classification performance was visualized in Fig. 6 using a technique we call Confusion Matrix Color Mapping (CM2). Here, every pixel in a binarized prediction image is colored according to its classification outcome in the binary confusion matrix, i.e., green for true positive, blue for false positive, and red for false negative pixels. Importantly, orange arrows indicate examples of grain boundaries
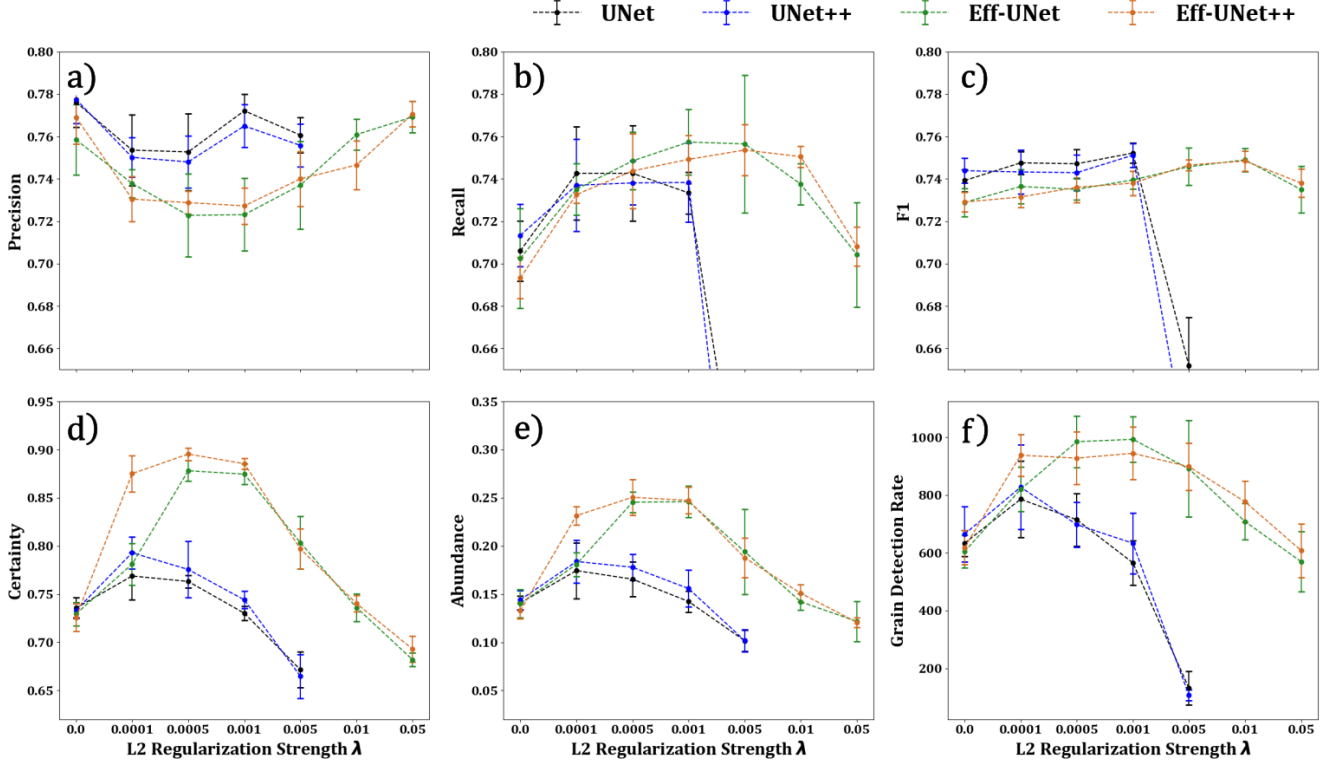
Figure 5. Metrics obtained from 5-fold cross-validation for λ optimization. Figs. a-c are classification metrics precision, recall, and F1-score respectively. Figs. d-e are proposed metrics certainty, abundance, and grain detection rate respectively. Error bars correspond to $\pm 1\sigma$

which were well-supported by the TEM image and were detected by the Eff-UNet model, but not present in the annotation. In other words, the human annotator missed these grain boundaries. Annotation errors act as a significant limitation of classification performance where good model predictions are incorrectly penalized, or where any attempt is bound to disagree.

To minimize loss, a model attempts to learn a set of operations that replicate the annotated grain boundaries like those in the middle column of Fig. 6. However, when true grain boundaries are mistakenly missing in the annotation, the model cannot rationalize these inconsistencies, potentially increasing model self-uncertainty. Any attempt to exactly fit these errors acts as a contradictory force to its typically well-supported operations. If annotation errors are interpreted by the model as high-level features with complex semantic content, the model could begin to overfit by trying to learn these features. The benefits of L2-regularization then become obvious: by constraining model complexity, it discourages fitting such annotation noise, and can instead help the model prioritize simpler, more reliable cues, thus reducing model self-uncertainty and promoting model self-confidence.

The theory above is supported well quantitatively. As shown in Fig. 5, without regularization all four architectures

have relatively high precision and low recall, meaning they guess less but are usually correct, and have very low prediction certainty and abundance. This indicates that they are skeptical. However, applying optimal L2-regularization, the architectures shift toward low precision and high recall, where they now guess more often and are less concerned with correctness. Certainty and abundance also increase substantially, suggesting less influence from human errors and more confidence with their predictions. Among all four architectures, Eff-UNet and Eff-UNet++ show the most significant improvement to prediction quality with grain detection rate reaching the highest observed levels, likely because of the greater capacity and redundancy supplied by EfficientNetB7.

4. Encoder Fine-Tuning

It has been shown that the performance of U-Net can be improved by using an EfficientNetB7 encoder pre-trained on ImageNet, with all weights unfrozen. However, it remains unclear whether performance gains stem from the Efficient-Net architecture itself, or from the benefits of pre-training and fine-tuning. To address this question, model performance was studied for various degrees of encoder fine-tuning and L2-regularization. Starting from a fully frozen encoder with ImageNet weights, the blocks of EfficientNet were progres-

| TEM Image | Annotation | CM2 Image |

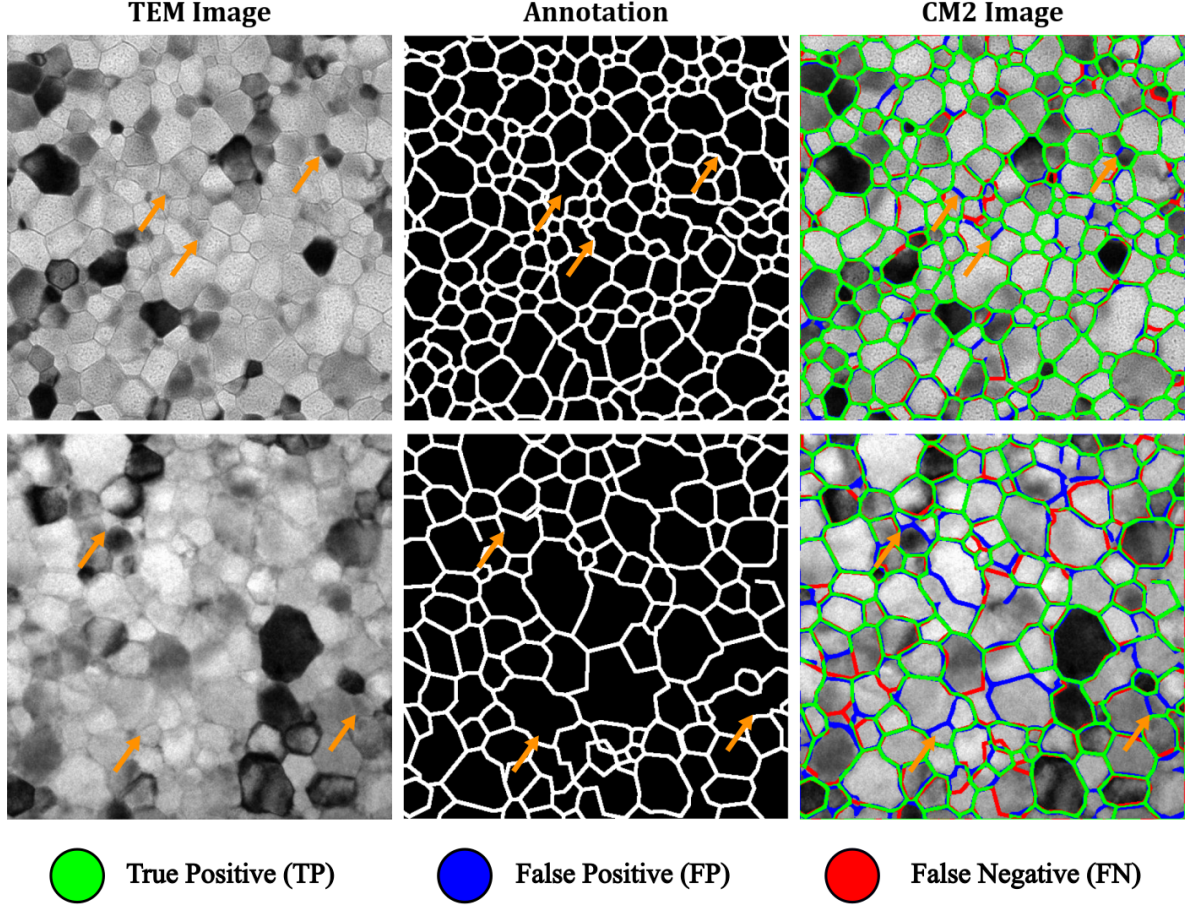● True Positive (TP) ● False Positive (FP) ● False Negative (FN)

Figure 6. Model predictions with Confusion Matrix Color Mapping (CM2) and their corresponding TEM image and annotation. Orange arrows indicate examples of annotations error. Predictions come the validation sets of Eff-UNet models with λ = 1e-3

sively unfrozen until all were trainable. To isolate the effect of pre-training, an additional condition was tested in which all weights were fully randomized and models were trained end-to-end. The evaluation results across these fine-tuning levels are summarized in Fig. 7, where the horizontal axes represent the degree of fine-tuning and the vertical axes are the metrics and their values. For each condition, 5-fold cross-validation was again used to obtain robust performance estimates. Additionally, three levels of L2-regularization (with λ=0, 1e-4, 1e-3) were applied to assess its potential influence on the observed trends.

According to Fig. 7, the first key observation is that when no fine-tuning is applied (i.e., left-most on the horizontal axes), models are skeptical with high precision, low recall, and low self-confidence. While increasing regularization leads to modest improvements, model self-confidence rises significantly only after unfreezing deeper encoder blocks. Second, all metrics roughly plateau once block 5 is unfrozen, with Fig. 7e showing the highest grain detection rate when λ = 1e-3. Third, when trained from scratch (i.e., right-most

on the horizontal axes), however, both certainty and abundance drop substantially. Furthermore, grain detection rate decreases by 20%. These results indicate pre-training is necessary for maximizing performance with EfficientNet encoders, and that fine-tuning the deepest layers leads to maximum confidence.

The trends seen in Fig. 7 provide some insight into the abilities of EfficientNet to adapt its pre-trained weights for a new task and dataset. The steep rise in performance as more blocks become trainable implies that the most important dissimilarity between ImageNet and the TEM dataset used in this work is the fine image structures. That is, most improvement comes from developing shallow layers responsible for extracting localized features. Although less significant quantitatively, developing deep layers which extract global features are crucial for building model confidence. This is most likely due to TEM images being much more homogeneous than natural scene images like those in ImageNet, and thus more suitable weights for global feature extraction must be learned [12].
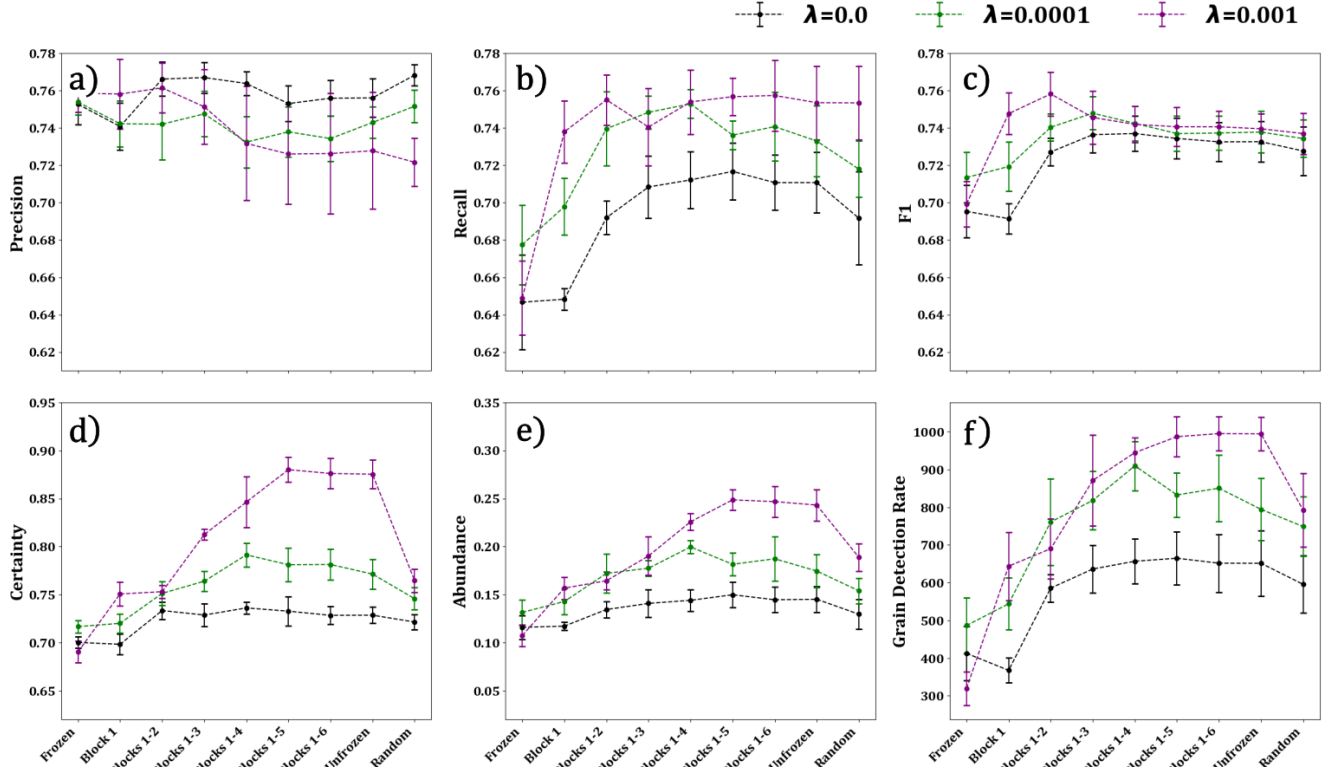
Figure 7. Metrics obtained from 5-fold cross-validation for fine-tuning optimization. The horizontal axis refers to which blocks of EfficientNetB7 (see Fig. 3) are unfrozen. "Frozen" refers to no fine-tuning and "Random" refers to no pre-training. Errors bars correspond to $\pm 1\sigma$

5. Conclusion

In this work, the performance of U-Net on a TEM image dataset of nanocrystalline grain morphologies has been improved by using a pre-trained EfficientNetB7 encoder with deep fine-tuning and L2-regularization. Two novel metrics, prediction certainty and abundance, have been introduced to provide a qualitative evaluation without regard a ground truth. A third metric, grain detection rate, was also used to provide a practical and holistic evaluation of model performance.

Replacing the encoder with EfficientNetB7 gave models excess capacity and redundancy, and by using L2-regularization, they obtained substantially higher prediction confidence. In total, 57% more grains were detected over the unregularized baseline U-Net architecture. To explain these benefits, it was proposed that regularization reduces model self-uncertainty by preventing overfitting of arbitrary human errors, but is only useful when a large pre-trained backbone is used.

A deeper dive into the importance of encoder pre-training was conducted as well, where it was found that model self-confidence is only acquired by fine-tuning the deepest layers which have been pre-trained on ImageNet. Some insight into

the dissimilarity between domain-specific and natural scene images used for training was discussed and it was concluded that there exists important differences at each spatial level during encoding. By fine-tuning all weights, responsible for extracting local and global features, model performance reaches its maximum.

Acknowledgments

Code and Data Availability

The code used in this work is located at https://github.com/psu-rdmap/unet-compare and can be used to train models on our dataset, or any other dataset with the allowable format. The data and analysis code, except for the model files due to size constraints, can be found on Zenodo with DOI 10.5281/zenodo.15626325.

References

[1] Khaled Alrfou, Amir Kordijazi, and Tian Zhao. Computer vision methods for the microstructural analysis of materials: The state-of-the-art and future perspectives. 2022. 1

[2] Waleed Alsabhan, Turky Alotaiby, and Basil Dudin. Detecting buildings and nonbuildings from satellite images using u-net. *Computational Intelligence and Neuroscience*, 2022:1–13, 2022. 1

[3] Gabriella Bruno, Matthew J Lynch, Ryan Jacobs, Dane D Morgan, and Kevin G Field. Evaluation of human-bias in labeling of ambiguous features in electron microscopy machine learning models. *Microscopy and Microanalysis*, 29: 1493–1494, 2023. 2

[4] Jia Deng, Wei Dong, Richard Socher, Li-Jia Li, Kai Li, and Li Fei-Fei. Imagenet: A large-scale hierarchical image database. In *2009 IEEE Conference on Computer Vision and Pattern Recognition*, pages 248–255. IEEE, 2009. 2, 3

[5] Ryan Jacobs. Deep learning object detection in materials science: Current state and future directions. *Computational Materials Science*, 211:111527, 2022. 1

[6] Zhenqing Liu, Yiwen Cao, Yize Wang, and Wei Wang. Computer vision-based concrete crack detection using u-net fully convolutional networks. *Automation in Construction*, 104: 129–139, 2019. 1

[7] Scott Mayer McKinney, Marcin Sieniek, Varun Godbole, Jonathan Godwin, Natasha Antropova, Hutan Ashrafian, Trevor Back, Mary Chesus, Greg S. Corrado, Ara Darzi, Mozziyar Etemadi, Florencia Garcia-Vicente, Fiona J. Gilbert, Mark Halling-Brown, Demis Hassabis, Sunny Jansen, Alan Karthikesalingam, Christopher J. Kelly, Dominic King, Joseph R. Ledsam, David Melnick, Hormuz Mostofi, Lily Peng, Joshua Jay Reicher, Bernardino Romera-Paredes, Richard Sidebottom, Mustafa Suleyman, Daniel Tse, Kenneth C. Young, Jeffrey De Fauw, and Shravya Shetty. International evaluation of an ai system for breast cancer screening. *Nature*, 577:89–94, 2020. 1

[8] Colin Ophus. Four-dimensional scanning transmission electron microscopy (4d-stem): From scanning nanodiffraction to ptychography and beyond. *Microscopy and Microanalysis*, 25:563–582, 2019. 1

[9] Olaf Ronneberger, Philipp Fischer, and Thomas Brox. U-net: Convolutional networks for biomedical image segmentation. 2015. 1

[10] Mingren Shen, Guanzhao Li, Dongxia Wu, Yuhan Liu, Jacob R.C. Greaves, Wei Hao, Nathaniel J. Krakauer, Leah Krudy, Jacob Perez, Varun Sreenivasan, Bryan Sanchez, Oigimer Torres-Velázquez, Wei Li, Kevin G. Field, and Dane Morgan. Multi defect detection and analysis of electron microscopy images with deep learning. *Computational Materials Science*, 199:110576, 2021. 1

[11] Mingren Shen, Guanzhao Li, Dongxia Wu, Yudai Yaguchi, Jack C. Haley, Kevin G. Field, and Dane Morgan. A deep learning based automatic defect analysis framework for in-situ tem ion irradiations. *Computational Materials Science*, 197:110560, 2021. 1

[12] Joshua Stuckner, Bryan Harder, and Timothy M. Smith. Microstructure segmentation with deep learning encoders pre-trained on a large microscopy dataset. *npj Computational Materials*, 8:200, 2022. 7

[13] Mingxing Tan and Quoc V. Le. Efficientnet: Rethinking model scaling for convolutional neural networks. 2019. 3

[14] Fabien H. Wagner, Alber Sanchez, Yuliya Tarabalka, Rodolfo G. Lotte, Matheus P. Ferreira, Marcos P. M. Aidar, Emanuel Gloor, Oliver L. Phillips, and Luiz E. O. C. Aragão. Using the u-net convolutional network to map forest types and disturbance in the atlantic rainforest with very high resolution images. *Remote Sensing in Ecology and Conservation*, 5:360–375, 2019. 1

[15] Chunshan Wang, Pengfei Du, Huarui Wu, Jiuxi Li, Chunjiang Zhao, and Huaji Zhu. A cucumber leaf disease severity classification method based on the fusion of deeplabv3+ and u-net. *Computers and Electronics in Agriculture*, 189:106373, 2021. 1

[16] David B. Williams and C. Barry Carter. *Transmission Electron Microscopy*. Springer US, 2009. 1

[17] Xinyuan Xu, Zefeng Yu, Wei-Ying Chen, Aiping Chen, Arthur Motta, and Xing Wang. Automated analysis of grain morphology in tem images using convolutional neural network with chac algorithm. *Journal of Nuclear Materials*, 588: 154813, 2024. 3

[18] Zefeng Yu, Xinyuan Xu, Wei-Ying Chen, Yogesh Sharma, Xing Wang, Aiping Chen, Christopher J. Ulmer, and Arthur T. Motta. In-situ irradiation-induced studies of grain growth kinetics of nanocrystalline uo2. *Acta Materialia*, 231:117856, 2022. 3

[19] Caixia Zhou, Yaping Huang, Mengyang Pu, Qingji Guan, Li Huang, and Haibin Ling. The treasure beneath multiple annotations: An uncertainty-aware edge detector. 2023. 2, 3

[20] Caixia Zhou, Yaping Huang, Mengyang Pu, Qingji Guan, Ruoxi Deng, and Haibin Ling. Muge: Multiple granularity edge detection. In *2024 IEEE/CVF Conference on Computer Vision and Pattern Recognition (CVPR)*, pages 25952–25962. IEEE, 2024. 2, 3

[21] Zongwei Zhou, Md Mahfuzur Rahman Siddiquee, Nima Tajbakhsh, and Jianming Liang. Unet++: A nested u-net architecture for medical image segmentation. 2018. 1